HAL
open science

# Fast cracks in high-speed photographs of shocked diamond

Geoffrey Willmott, John Field

## To cite this version:

Geoffrey Willmott, John Field. Fast cracks in high-speed photographs of shocked diamond. Philosophical Magazine, 2006, 86 (27), pp.4305-4318. 10.1080/14786430500482336 . hal-00513642

**HAL Id: hal-00513642**

**https://hal.science/hal-00513642v1**

Submitted on 1 Sep 2010

**HAL** is a multi-disciplinary open access archive for the deposit and dissemination of scientific research documents, whether they are published or not. The documents may come from teaching and research institutions in France or abroad, or from public or private research centers.

L'archive ouverte pluridisciplinaire **HAL**, est destinée au dépôt et à la diffusion de documents scientifiques de niveau recherche, publiés ou non, émanant des établissements d'enseignement et de recherche français ou étrangers, des laboratoires publics ou privés.

# Fast cracks in high-speed photographs of shocked diamond

| | |
|---|---|
| Journal: | *Philosophical Magazine & Philosophical Magazine Letters* |
| Manuscript ID: | TPHM-05-Mar-0066.R2 |
| Journal Selection: | Philosophical Magazine |
| Date Submitted by the Author: | 29-Sep-2005 |
| Complete List of Authors: | Willmott, Geoffrey; University of Cambridge, Physics<br>Field, John; University of Cambridge, Physics |
| Keywords: | high-speed photography, diamond, cracks |
| Keywords (user supplied): | |
| | |
| Note: The following files were submitted by the author for peer review, but cannot be converted to PDF. You must view these files (e.g. movies) online. | |
| CracksPaper.tex | |

scholarONE™
Manuscript Central

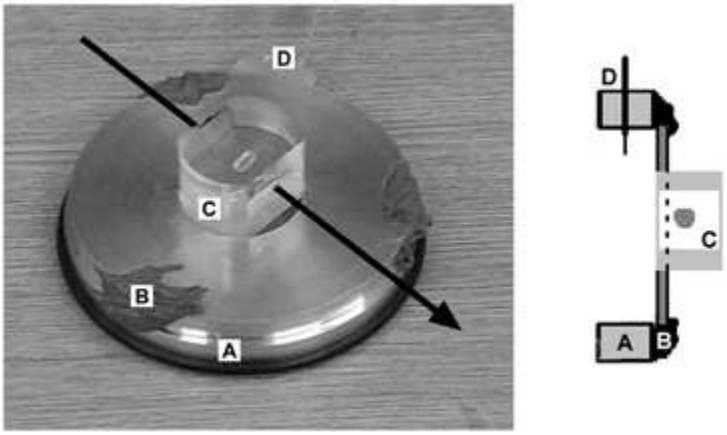


130x77mm (72 x 72 DPI)

er Review Only

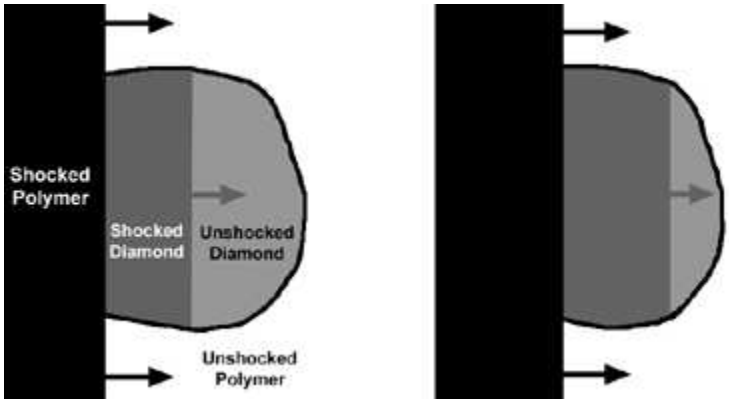


130x69mm (72 x 72 DPI)

For Review Only

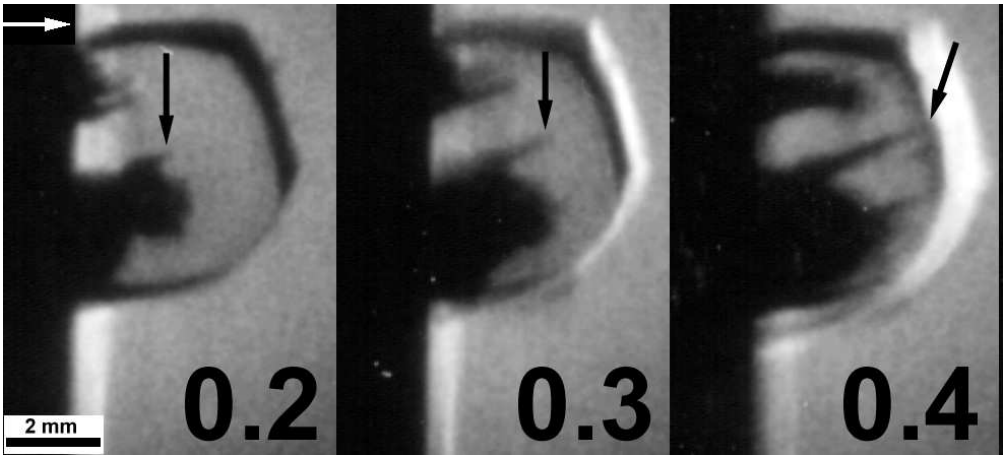


347x156mm (72 x 72 DPI)

er Review Only

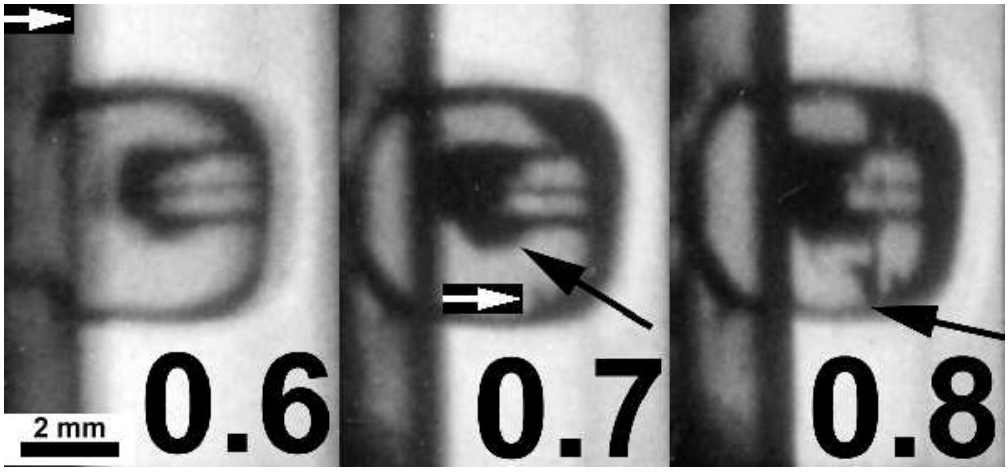


211x98mm (72 x 72 DPI)

For Review Only

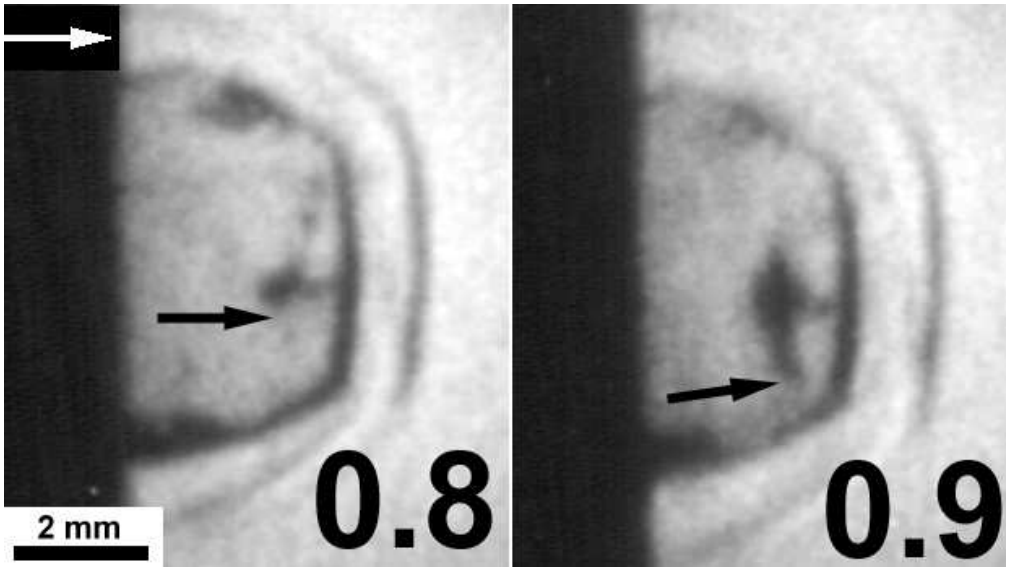


217x122mm (72 x 72 DPI)

For Review Only

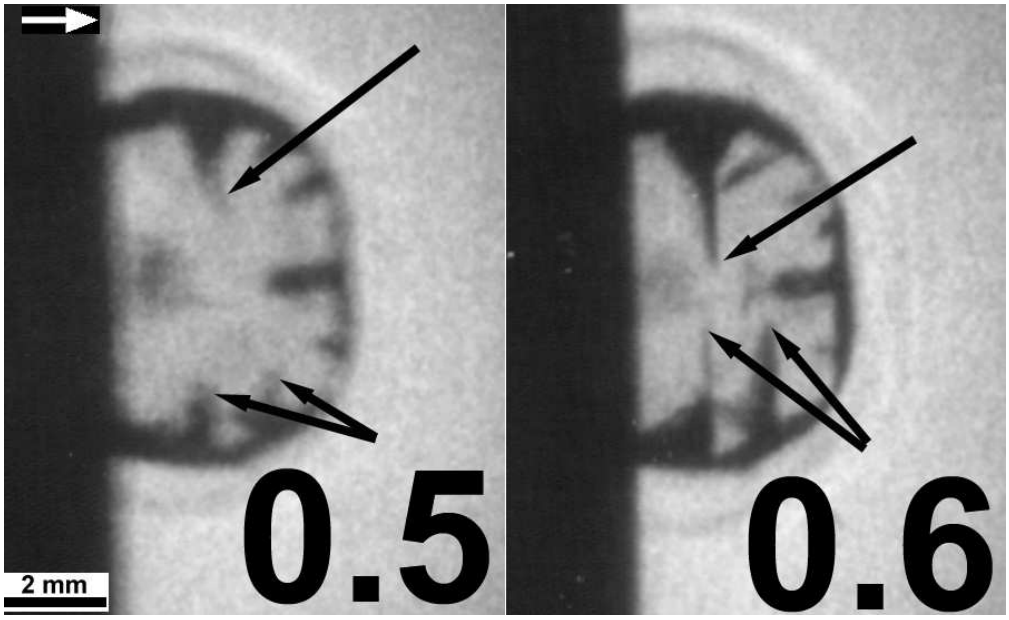


317x194mm (72 x 72 DPI)

Review Only

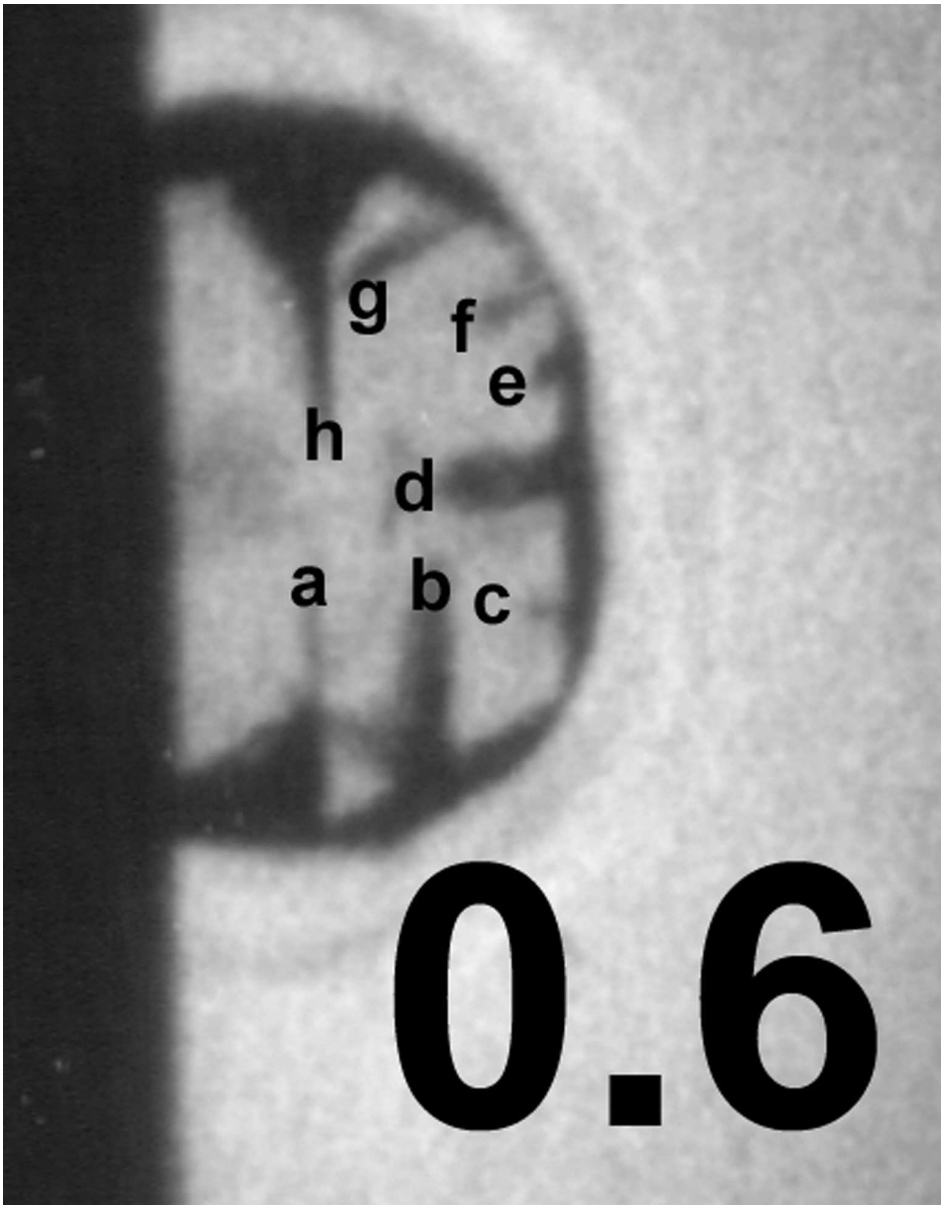


130x166mm (600 x 600 DPI)

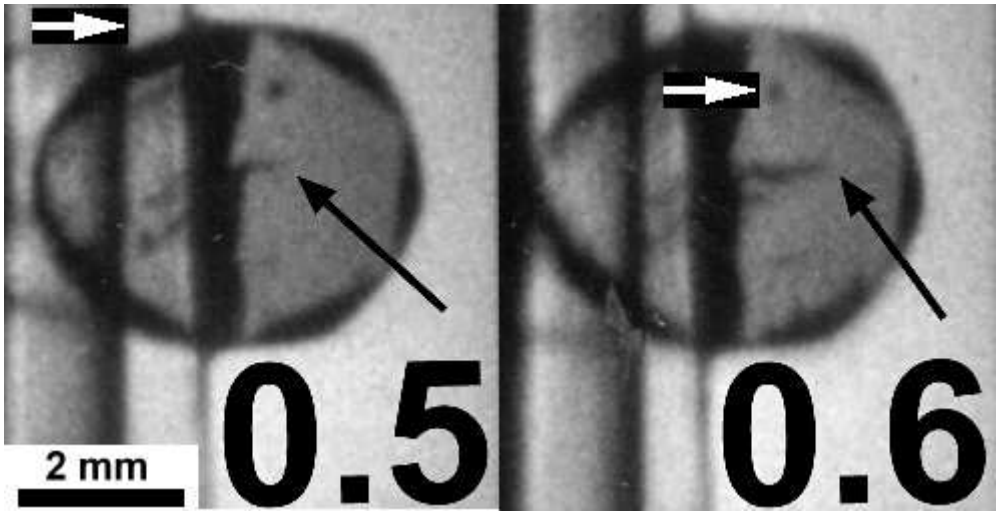


174x89mm (72 x 72 DPI)

Review Only

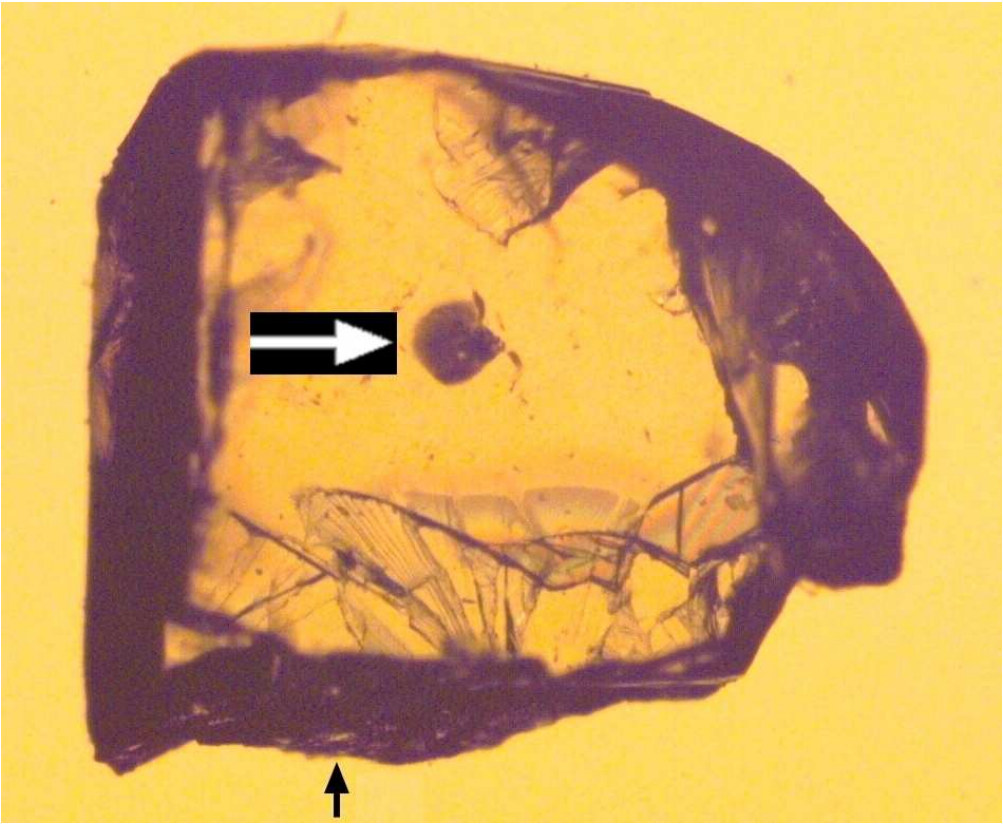

334x274mm (72 x 72 DPI)

w Only

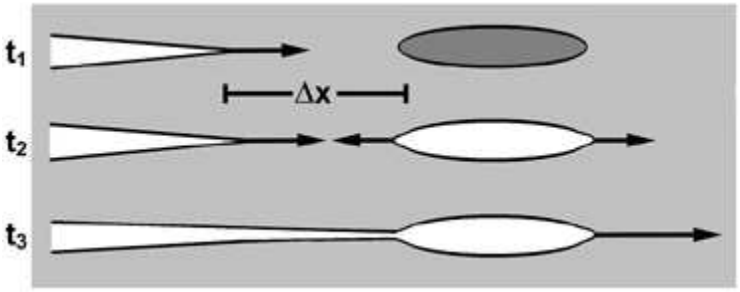


130x55mm (72 x 72 DPI)

Peer Review Only

# Fast cracks in high-speed photographs of shocked diamond

G. R. Willmott and J. E. Field

Physics and Chemistry of Solids, Cavendish Laboratory,

Madingley Rd, Cambridge CB3 0HE, UK

Phone: (44) (0)1223 339375

Fax: (44) (0)1223 350266

Email: grw23@cam.ac.uk

For Peer Review Only

Six fracture surfaces have been observed extending at velocities between $c_R$ (the Rayleigh wave velocity) and $1.3c_R$ in high-speed photographs of four diamond specimens. The diamonds were embedded in a transparent polymer and shocked in plate impact experiments. The measured velocities exceed limiting velocities proposed in theoretical and practical studies of single mode I cracks in diamond. The fracture surfaces probably extend by initiation and coalescence of multiple tensile fractures along a single cleavage plane. This mechanism is dependent on the suppression of cracks branching from the {111} growth plane in diamond and considers the population of flaws near a propagating crack tip.

Keywords: Diamond; Cracks; High-speed photography

# 1 Introduction

Analysis of the onset of brittle fracture began with Griffith's seminal paper, in which the tensile stress required to extend an ideal single crack in an isotropic brittle solid was derived [1]. Griffith's approach, which considered mechanical and free surface energies, has been used to describe brittle fracture in numerous and varied applications [2]. Mott [3] extended Griffith's work to the analysis of propagating cracks by considering kinetic energy. Theoretical analyses of brittle fracture have since focussed on crack propagation in solids that have a linear elastic constitutive response up to failure (perfectly brittle) and are isotropic and homogeneous (monolithic) in terms of constitutive response and fracture toughness. This mathematically complex topic has been dealt with at length in modern summaries by Broberg [4] and Freund [5].

A common feature of analytic solutions for single mode I cracks is that the crack velocity ($v$) approaches asymptotically the Rayleigh (surface) wave velocity ($c_R$), which is ~90 % of the shear wave velocity ($c_S$) and significantly less than the longitudinal wave velocity ($c_L$). It seems physically reasonable that the speed of a crack should be limited by the speed at which waves can propagate along the free surface it creates. This limit has been verified in experiments using various techniques (including high-speed photography) to record crack velocities in a variety of materials [6]. Cracks were observed propagating at up to $0.88c_R$ along a preferred cleavage plane in magnesium oxide. In general, single tensile cracks run at velocities up to a practical limit of $\sim 0.6c_R$, at which point branching occurs.

Experiments in isotropic materials (e.g. [7]) have shown that cracks are most easily initiated and propagate preferentially along pathways for which the stress at the crack tip is purely tensile. In an anisotropic material, pure mode I crack propagation can be energetically unfavourable, in which case a crack can propagate with mixed-mode loading. The problem of mode II cracks moving along predetermined



For Peer Review Only

weak paths has been a subject of some interest over the past decade due to the development of specialized, inhomogeneous engineering materials and geophysical reports of 'intersonic' average fault plane rupture velocities [8]. For an intersonic crack, $c_S < v < c_L$, Rosakis et al. [9] have observed intersonic mode II fractures on a weakened plane in a polymer using high-speed photography and a dynamic photoelasticity technique. The cracks were accompanied by multiple conchoidal fractures in directions perpendicular to the crack path.

Rosakis [7] has reviewed the phenomenon of intersonic shear rupture along a predetermined weak plane in an otherwise monolithic material. There is a singular analytic solution for the stress field at the tip of a mode II intersonic crack [10]. The physical implication of this solution is that shear cracks should be able to propagate at $v = \sqrt{2}c_S$. Analytical and modelling studies which incorporate non-steady-state solutions with finite process zones have described possible mechanisms for shear cracks propagating at speeds greater than $c_S$ other than $\sqrt{2}c_S$. The Burridge-Andrews mechanism has become widely accepted due to corroborating results from other numerical studies [7].

Griffith [1] also noticed that flaw populations have a significant effect on the strength of apparently perfect materials. In tension, flaws will evolve into cracks if they are large or located in regions where the stresses are large. Any macroscopic specimen of a brittle material contains a microscopic population of flaws. The genesis, size and distribution of flaws in brittle solids have been discussed by Lawn [2].

The current paper reports experimental measurements of fracture velocities from well-calibrated high-speed photographic sequences of shocked diamond. The implications of these measurements, in which some cracks appear to move faster than $c_R$, are interpreted in the context of previous work. Due consideration is given to the role of flaws that lie near a propagating crack tip in a real material. A mech-



For Peer Review Only

anism for extension of fracture surfaces in tension at velocities greater than $c_R$ is described.

Diamond has an extremely stable covalent lattice that is responsible for many extreme physical characteristics, making it suitable for a wide range of industrial and technological applications. It is often considered 'perfectly brittle', so it is the ideal material to compare with analytical approaches to fracture mechanics. The anisotropy of diamond, in which the {111} crystallographic plane dominates cleavage, suppresses crack branching and encourages propagation of high velocity cracks. Field [6] has previously measured a crack velocity of 7.2 mm µs$^{-1}$ ($0.7c_R$) in high-speed photographs of diamond. A limited number of specimens were used and Field noted that the maximum velocity for cracks in diamond could be higher.

## 2 Experimental

### 2.1 *Diamond*

[Insert table 1 about here]

Diamond is a form of pure elemental carbon in which each atom has four tetrahedral sp$^3$ bonds with its nearest neighbours. The diamond lattice has a high coordination number (4), strong bonds, short bond length (0.154 nm) and a stable structure. Pure diamond is transparent in optical light. Other physical properties are summarized in table 1. Field and Freeman's [11] experimental value of $\gamma_{111}$ from indentation is $5.50 \pm 0.15$ J m$^{-2}$, and close enough to theory to suggest that plastic deformation at the crack tip is negligible. A summary of research into the strength, fracture and erosion properties of diamond has been compiled by Field [12].

Most natural diamonds grow by deposition of successive layers on {111} facets, so that the shape of recovered diamonds is that of interlinking {111} planes: an



For Peer Review Only

octahedron. The {111} crystallographic plane is the dominant cleavage plane in diamond, as first noted by Ramaseshan [13]. A static crack on a {111} plane will not extend on a different crystallographic plane, regardless of the loading conditions applied [14]. A first-principles quantum mechanical approach [15] has shown that the tensile strength of a perfect diamond crystal is lowest in the ⟨111⟩direction. Flaws and inclusions that encourage cleavage are likely to lie on growth planes; the tensile strength derived from indentation experiments (table 1) is a factor of 50 less than theoretical calculations.

By taking into account the crystallographic variation of elastic moduli in diamond and possible confinement states, extreme values of $c_L$ and $c_S$ in diamond have been calculated. The range of possible values is 17.3–19.5 mm µs$^{-1}$ for $c_L$ and 10.5–13.0 mm µs$^{-1}$ for $c_S$. Viktorov [16], who has given a full description of Rayleigh waves, suggests the following approximate formula for calculation of $c_R$:

$$c_R = \left(\frac{0.87 + 1.12\nu}{1 + \nu}\right) c_S \tag{1}$$

Considering the full range of possible values for $c_S$ and $\nu$, $c_R$ can take a range of values between 9.6 and 11.4 mm µs$^{-1}$. Applied hydrostatic [17] or shock [18] compression can also alter the elastic properties of a material. Under shock conditions similar to those in the current experiments, $c_L$ does not increase by more than 15 % from the ambient value in metallic solids.

### 2.2 *High-Speed Photography*

High-speed photography is probably the most data-rich diagnostic technique for shock events involving transparent materials. High-speed cameras capture photographs, or 'frames', in time-ordered sequences. The image in each frame is generated using light that enters the camera during the exposure time for that frame. The interframe time (IFT) is the interval between the start of successive exposures.



For Peer Review Only

Modern summaries of the history and applications of high-speed photography have been compiled by Field [19] and Ray [20].

An image-converter camera, the IMCO Ultranac 501, was used in the current research. This camera can produce between 8 and 24 frames at framing rates up to 2 x $10^7$ $s^{-1}$, with a minimum exposure time of 10 ns. The IFT and exposure time are fully programmable for each frame. Images are produced as good-quality Polaroid prints.

In the current study, black and white photographs of shock waves and fracture in transparent brittle solids are of interest. In a uniformly illuminated transparent material, a shock front is imaged as a dark line due to a shock-induced discontinuity in the refractive index across the wave front ('Schlieren' contrast). A fracture is imaged as a dark line once the crack is wider than half the wavelength of the illuminating light, or 200–350 nm for white light. If a fracture plane is parallel to the angle of view, the crack will appear sharp; thicker fractures lie on oblique angles. Cracks sometimes 'disappear' in high-speed sequences when fracture surfaces are pushed together [21].

### 2.3 *Embedded Diamond Experiments*

An experimental technique was developed in order to view the effects of shock waves on transparent diamond specimens. Nine specially prepared, polished slices of type IaA diamond (diameter ∼5 mm and thickness 1–2 mm) were made available for the current study [14]. Specimens were either 'good quality' (containing no macroscopic flaws) or 'cracked' (with visible fracture surfaces). Each diamond was embedded in a matrix of polymethylmethacrylate (PMMA), which was synthesized by heating and pressing a powder. The uniform pressure applied to the powder was 0.02 GPa and the polymer was cooled slowly to avoid trapping internal stresses.

[Insert figure 1 about here]



For Peer Review Only

Planar shock waves were induced in the PMMA blocks using the plate impact technique in the single-stage light gas gun at the Cavendish Laboratory [22]. Target geometry is shown in figure 1. Target and flyer plates were machined flat and parallel to within ± 5 $\mu$m. At impact, the plates are aligned to within ± 0.5 mrad using a mechanical alignment dial gauge. Copper flyer plates of thickness 3 mm were mounted on polycarbonate sabots, with a recess behind each flyer plate providing a free rear surface. A series of shorting pins and a specially designed 'make' trigger were used to trigger diagnostics precisely and measure impact velocity (accurate to within ± 0.5 %) for each experiment. Shock waves had a 'top hat' profile, with duration determined by the thickness of the flyer plate and the well-known velocity of shock waves in copper.

When the shock wave reached the embedded disc, high-speed photographs were taken. Each embedded particle had polished faces normal to the line-of-sight of the camera. The sides of each polymer plate were flattened and polished parallel to the particle faces so that light entering the camera was not significantly refracted by the transparent solids. Therefore, the diamonds were fixed in a carefully aligned, mounted position, in order to allow the camera and flash to be triggered with high precision.

[Insert figure 2 about here]

Photographic images of the embedded diamonds are obscured by the shock wave in the PMMA matrix. However, the shock wave travels much faster through the diamond ($c_L$ = 17.5 mm µ s$^{-1}$) than the PMMA ($c_L$ = 2.6 mm µ s$^{-1}$). An area ('window') of shocked diamond is visible in the interval immediately after the shock wave entered each diamond specimen (figure 2).

High time resolution was required because a window is imaged for less than 5 µs. A shock wave travels through 5 mm of diamond in ∼300 ns, so an IFT of 100 ns with 50 ns exposure time was used. Interframe and exposure times were carefully



For Peer Review Only

verified to within ± 2 ns using the Ultranac 501's electronic shutter monitor [14]. Each sequence consisted of 18 frames. Reliability of the technique was paramount, so it was developed using embedded glass and sapphire particles [14].

Lighting is an important consideration for photography at high framing rates. A reusable arc-discharge lamp was placed behind the specimen (back-lighting), in the line of sight of the camera lens. The lamp discharged 2 kV across a 40 µF capacitor in ∼10 µs. The rise time was consistently 2–3 µs and the total output from a single flash was 80 J. Sheets of semi-transparent paper were placed between the flash and the specimen to diffuse the light.

Impact was viewed through a clear glass portal in the side of the gas gun's impact chamber. The distance between the lens and the specimen was ∼1 m. The lens aperture was opened as widely as possible in order to maximise light entering the camera, as long as the depth of field did not become too small.

High-speed photographs were digitized and spatially calibrated using photographs of the specimens that were taken prior to each experiment. Uncertainties in crack velocity measurements reflect errors in spatial and temporal calibration. Velocity measurements represent a lower bound on actual crack speed, because fracture surfaces can have a directional component perpendicular to the two-dimensional image in the high-speed photographs. Additionally, a crack might only extend during part of the 50 ns exposure time for each frame.

## 3 Results

[Insert table 2 about here]

[Insert figure 3 about here]

Figure 3 shows high-speed photographic frames from four embedded diamond experiments (table 2). Labels on photographs indicate the time in microseconds after the shock wave reached the embedded particle ('shock wave arrival'). The shock



For Peer Review Only

wave travelling through the PMMA is imaged as a thick dark line moving from left to right and extending vertically from the top to the bottom of each frame, obscuring the embedded particle. The shock wave within the diamond traverses the specimen approximately 3 times in 1 µs, by which time the shock in the PMMA obscures roughly half the specimen. When the shock wave in the diamond first reaches the back (right) edge of each specimen, ∼0.3 µs after shock wave arrival, a 'bow wave' is imaged moving into the surrounding matrix material. The specimens are too thin for shock waves to be observed in the diamond itself.

[Insert table 3 about here]

Average crack velocities from experiment D5 are recorded in table 3. Labels for these cracks are indicated in figure 3. The cracks extend in three dimensions and do not necessarily propagate throughout the exposure time for each frame. The tabulated measurements are averaged across the interframe time, and therefore represent a lower bound on the maximum crack velocity. The values in table 3 are typical of crack velocities measured in the embedded particle experiments. The velocity of individual cracks can vary significantly as a function of time. Cracks propagated at speeds ranging from less than 3 mm µs$^{-1}$ to greater than the Rayleigh wave velocity ($c_R$). The latter are the subject of the discussion.

Table 4 records the average velocities of the fastest cracks ($v \gtrsim c_R$) measured from high-speed photographs. Growth of these cracks is indicated by black arrows in figure 3. All of the cracks initiated within 0.5 µs of shock wave arrival, except cracks 2a and 3a, and all of the cracks propagate along {111} cleavage planes. Other, relatively fast cracks ($v \gtrsim 0.8c_R$) were observed in specimens D3 and D5.

[Insert table 4 about here]

[Insert figure 4 about here]

Figure 4 provides evidence that the growing dark lines observed in photographic sequences should be identified as fracture surfaces. In figure 4(a), arrows denote



For Peer Review Only

a crack propagating from the crystal centre of a semi-embedded diamond particle in experiment D8. The crack moves along a {111} plane at an average velocity of $8.4 \pm 2.4$ mm µs$^{-1}$, slower than the cracks recorded in table 4. A 31 mg fragment recovered from experiment D8 (figure 4(b)) can be directly linked with the original specimen due to the central, near-circular inclusion that is indicated by white arrows in figures 4(a) and 4(b). In figure 4(b), the fracture surface denoted by the arrow was formed by the crack in figure 4(a). Fracture surfaces of all recovered diamond fragments have been analysed in detail [14], but provide little insight into the mechanism of fast crack growth.

# 4 Discussion

Crack velocities in table 4 are between 2 and 37 % greater than $c_R$ for the case when $c_R = 10.3$ mm µs$^{-1}$. Crack velocities greater than $0.9c_R$ have not been observed for single mode I cracks in diamond or other materials [6]. Mode II cracks on a weakened plane in a polymer [9] and cracks driven by pressurised fluid expansion at the crack tip in sodium chloride [23] have been observed growing faster than $c_R$. In the current research, high-speed cracks predominantly occurred when the impact velocity was relatively high, so that large stresses were induced throughout the diamond.

## 4.1 *Multiple Initiation Mechanism*

The most likely explanation for the elevated crack speeds observed in the current experiments is a 'multiple initiation' mechanism (figure 5). This mechanism accounts for the presence of flaws near a crack tip in a real material. If the time $(t_3 - t_1)$ and length $(\Delta x)$ scales defined in figure 5 are smaller than the experimental resolution, the fracture surface will appear to grow as a single, fast-moving crack. Experiments carried out by Ravi-Chandar and Knauss [26] concluded that



For Peer Review Only

brittle fracture could occur by way of a similar mechanism, involving coalescence of microcracks.

[Insert figure 5 about here]

The value of $\Delta x$ can be constrained using high-speed photographs. In the case of crack 3a (figure 3(c)), the fracture appears to grow from the developing central region (as indicated by the black arrows) as well as from a feature neat the edge of the disc, denoted by a white arrow in the frame 0.7 µs after shock wave arrival. The features at either end of the eventual fracture are ∼2 mm apart and join up in the 100 ns separating the frames 0.7 and 0.8 µs after shock wave arrival. The other fast cracks appear to propagate in a single direction; cracks 1a (figure 3(a)) and 5h (figure 3(d)) do so over three frames. The upper limit of $t_3 - t_1$ is the interframe time, 100 ns. The limiting velocity for single cracks restricts $\Delta x$ to less than 2 mm. Microscopic flaws incorporated during octahedral growth commonly populate {111} planes in diamond, and flaws large enough to produce clearly visible birefringence fringes occur with a frequency of approximately 10 mm$^{-2}$ on natural diamond surfaces [24]. It is likely that multiple initiation occurs on microscopic scales. The proposed mechanism does not require that secondary flaws lie near specimen surfaces, where flaws in crystal specimens are most prevalent. Secondary fractures in crack 1a and the cracks in specimen D5 would initiate a significant distance from specimen edges.

In isotropic materials, it is energetically favourable for fast cracks to 'branch' into the plane on which tensile stress is maximized, which lies at a finite angle to the original crack plane [5]. When conditions are almost conducive to crack branching, microcracks can initiate ahead of the crack tip without extending into a full crack branch, forming a roughened texture on the fracture surface [6]. Full crack branches are therefore generated by secondary fractures ahead of the crack tip. This mechanism is identical to the multiple initiation mechanism except that, in



For Peer Review Only

diamond, preference for {111} cleavage suppresses branching fractures and restricts secondary fractures to the {111} cleavage planes.

On a single weak cleavage plane containing particularly large flaws, abundant flaws and / or significant internal stresses, multiple fractures could be nucleated independently. Alternatively, if the stress field near the tip of a secondary flaw is intensified by the propagating primary crack, multiple fractures could be linked. Stress intensification would be caused by the stress field surrounding the tip of the primary crack, or stress waves radiating from the propagating primary crack tip. Linked initiation is more likely when $\Delta x$ is small.

Secondary initiation preferentially occurs on the same cleavage plane as the primary fracture. If this was not the case, multiple fractures would be observed on {111} planes adjacent to secondary fractures, or conchoidal fracture would be required to join primary and secondary fractures on separate cleavage planes. Neither phenomenon is observed in the high-speed photographs. This observation requires that, if secondary initiation is independent, the cleavage plane of a fast crack must be particularly weak in comparison with nearby cleavage planes. If secondary initiation is linked, the energetic expense of conchoidal fracture requires that secondary cracks lie on the same cleavage plane as the primary crack.

Further experimental observations of cracks in isotropic materials are consistent with the multiple initiation mechanism. Crack branching in isotropic materials is dependent on flaws lying within the stress field surrounding the crack tip [6], as is the case with diamond. Increased loading results in more frequent crack branching in isotropic materials [6]; when branching is suppressed, increased loading produces higher crack velocities (as observed in the current study) due to more frequent secondary fracture. A very similar phenomenon to the multiple initiation mechanism is observed in high-speed photography of glass rod impact experiments [25], when secondary fractures are sometimes observed further from the impact



For Peer Review Only

plane than the failure front.

The multiple initiation mechanism is similar to the Burridge-Andrews mechanism for intersonic mode II shear cracks [7]. Burridge [27] found a peak in the analytical shear stress field propagating slightly ahead of a mode II crack tip at speeds close to $c_R$. Working independently with a numerical finite-difference scheme, Andrews [28] found that a secondary slip region nucleates ahead of the crack under similar conditions. New fractures coalesce with the original crack and the fracture surface can extend intersonically.

In both the Burridge-Andrews and multiple initiation mechanisms, fracture is confined to a single plane by material anisotropy and secondary fractures nucleate ahead of a propagating crack tip. However, multiple initiation requires stress intensification at flaws ahead of the crack tip whereas the stress field near the tip of a mode II crack has an intrinsic local maximum. Neither mechanism strictly describes propagation of a single (primary) crack, but both explain experimental observations of fracture surfaces that extend at a rate that is faster than $c_R$.

The two mechanisms blur the distinction between single and multiple cracks. Classification of real single cracks depends on the characteristic length scales of non-idealities (e.g. flaws) in real materials. These length scales (relative to crack velocity) are typically too small for multiple cracks to be resolved in experiments.

### 4.2 *Other Possible Explanations*

It is unlikely that the fast cracks in the current research extend by way of a predominantly mode II (shearing) mechanism. They constitute a significant fraction of all the macroscopic cracks observed in experiments D1, D2, D3 and D5; cracks preferentially nucleate in pure tension. The cracks propagate in multiple directions in individual specimens, rather than a particular direction favoured by macroscopic shear stress. There is no evidence of conchoidal fracture accompanying the fast



For Peer Review Only

cracks, unlike the fast mode II fractures observed by Rosakis [7].

Cracks are only imaged once they have opened a distance equal to half the wavelength of the illuminating light. A crack could erroneously appear to travel at an elevated velocity if the opening angle near the crack tip varied significantly over time scales comparable to the IFT. Considering the specimen brittleness, image resolution and short IFT in the current experiments, such variation is unlikely to be significant.

The propagating fractures could be single mode I cracks moving faster than the theoretical limiting speed under linear elastodynamics ($\sim c_R$ [5, 7]). The effects of the zone of plastically deformed material present at any real crack tip are not well understood. However, diamond is highly brittle, so any disparity between the theory for single cracks and the current observations is more likely to be caused by experimental conditions than any theoretical shortcomings.

## 5 Conclusions

Well-calibrated high-speed photographs have been used to observe six fracture surfaces extending at velocities between $c_R$ and $1.3c_R$ in shocked diamond. These velocities are higher than the limiting velocities previously proposed in theoretical and practical studies of single mode I cracks in diamond and other material.

The most likely explanation for the fast crack measurements has been explained using a multiple initiation mechanism. In this mechanism, single cracks coalesce with secondary cracks on the same cleavage plane in an anisotropic material. The coalescence is not observed in experiments due to resolution limits and the fracture surface appears to extend faster than the speed of a single crack. Multiple initiation is identical to the mechanism that causes crack branching in an isotropic material, except that secondary fractures ahead of the crack tip are restricted to the same cleavage plane as the initial crack. This mechanism is also consistent with high-



For Peer Review Only

speed photography of shocked glass and previous experimental studies of single crack propagation.

The multiple initiation mechanism has many similar features to the Burridge-Andrews mechanism, which is widely used to describe fast mode II crack propagation. It is apparent that analyses of single cracks are restricted by the effects of flaws in real materials and the limits of resolution in experimental diagnostics.

## 6 Acknowledgements

The authors thank Dr. Alan Guest and De Beers Consolidated Mines Ltd. for support of this research. Specimens were prepared by Ray Flaxman and Daniel Cross. High-speed photography at the Cavendish Laboratory is funded by the Engineering and Physical Sciences Research Council.

## References

[1] A. A. Griffith, Phil. Trans. R. Soc. Lond. A, **221** 163 (1920).

[2] B. R. Lawn, *Fracture of Brittle Solids*, 2nd edition (Cambridge University Press, Cambridge, 1993).

[3] N. F. Mott, Engineering **165** 16 (1948).

[4] K. B. Broberg, *Cracks and Fracture* (Academic Press, London, 1999).

[5] L. B. Freund, *Dynamic Fracture Mechanics* (Cambridge University Press, Cambridge, 1990).

[6] J. E. Field, Contemp. Phys. **12** 1 (1971).

[7] A. J. Rosakis, Advances in Physics **51** 1189 (2002).



For Peer Review Only

[8] M. Bouchon, M. P. Bouin, H. Karabulut, N. Toksoz, M. Dietrich and A. J. Rosakis, Geophys. Res. Letts. **28** 2723 (2001).

[9] A. J. Rosakis, O. Samudrala and D. Coker, Science **284** 1337 (1999).

[10] L. B. Freund, J. Geophys. Res. **84** 2199 (1979).

[11] J. E. Field and C. J. Freeman, Phil. Mag. A **43** 595 (1981).

[12] J. E. Field, Chapter 12 in *The Properties of Natural and Synthetic Diamond*, edited by J. E. Field (Academic Press, London, 1992).

[13] S. Ramaseshan, Proc. Indian Acad. Sci. **A24** 114 (1946).

[14] G. R. Willmott, *Shock studies of kimberlite, diamond and brittle embedded particles*. PhD thesis, University of Cambridge (2004).

[15] R. H. Telling, C. J. Pickard, M. C. Payne and J. E. Field, Phys. Rev. Lett. **84** 5160 (2000).

[16] I. A. Viktorov, *Rayleigh and Lamb Waves: Physical Theory and Applications* (Plenum Press, New York, 1967).

[17] F. F. Voronov and L. F. Vereshchagin, Phys. Metals Metallog. **11** 111 (1961).

[18] T. S. Duffy and T. J. Ahrens, J. Geophys. Res. **97** 4503 (1992).

[19] J. E. Field, Proc. R. Institution **60** 195 (1988).

[20] S. F. Ray, *High Speed Photography and Photonics* (Focal Press, London, 1997).

[21] F. P. Bowden and J. E. Field, Proc. R. Soc. Lond. A **282** 331 (1964).

[22] N. K. Bourne, Z. Rosenberg, D. J. Johnson, J. E. Field, A. E. Timbs and R. P. Flaxman, Meas. Sci. Technol. **6** 1462 (1995).

[23] S. Winkler, D. R. Curran and D. A. Shockey, Int. J. Fracture **6** 271 (1970).



For Peer Review Only

[24] A. R. Lang, Nature **213** 248 (1967).

[25] G. R. Willmott and D. D. Radford, J. Appl. Phys. **97** 093522 (2005).

[26] K. Ravi-Chandar and W. G. Knauss, Int. J. Fract. **25** 247 (1984).

[27] R. Burridge, Geophys. J. Royal Astronom. **35** 439 (1973).

[28] D. J. Andrews, J. Geophys. Res. **81** 5679 (1976).

For Peer Review Only

Table 1: Physical characteristics of diamond [12]. The values for Young's modulus ($E$) and Poisson's ratio ($\nu$) correspond, respectively, to $E_{111}$ and the 'isotropic aggregate value' of $\nu$ [12]. Wave velocity values correspond to a state of uniaxial strain in which the tabulated values of $E$ and $\nu$ are used in calculations. Variation of these values is discussed in the text.

| | | |
|---|---|---|
| Density | $\rho_0$ | 3.52 g cm$^{-3}$ |
| Young's Modulus | $E$ | 1050 GPa |
| Poisson's Ratio | $\nu$ | 0.07 |
| Longitudinal Elastic Wave Velocity | $c_L$ | 17.5 mm µ s$^{-1}$ |
| Transverse Elastic Wave Velocity | $c_S$ | 11.6 mm µ s$^{-1}$ |
| Rayleigh Wave Velocity | $c_R$ | 10.3 mm µ s$^{-1}$ |
| Practical Tensile Strength | $\sigma_f$ | 3.75 GPa |
| Theoretical Fracture Surface Energy | $\gamma_{111}$ | 5.3 J m$^{-2}$ |
| Critical Stress Intensity Factor | $K_{IC}$ | 3.4 MN m$^{-\frac{3}{2}}$ |
| Refractive Index | $n$ | 2.417 |



For Peer Review Only

Table 2: Summary of the conditions for the five impact experiments cited in this paper.

| Experiment | Impact Velocity | Specimen Details | | |
|---|---|---|---|---|
| | (mm µs$^{-1}$) | Plane of Slice | Quality | Mass ($\pm$ 1 mg) |
| D1 | $506 \pm 3$ | {110} | Cracked | 126 |
| D2 | $503 \pm 3$ | {110} | Clean | 168 |
| D3 | $296 \pm 1$ | {100} | Cracked | 208 |
| D5 | $407 \pm 2$ | {111} | Clean | 156 |
| D8 | $453 \pm 2$ | {111} | Cracked | 148 |

For Peer Review Only

Table 3: Crack propagation velocities for the eight cracks from experiment D5, as labelled in figure 3(e).

| | Average Crack Velocity (mm µs$^{-1}$) in Time Interval | | | | |
|---|---|---|---|---|---|
| Crack | 0.2–0.3 µs | 0.3–0.4 µs | 0.4–0.5 µs | 0.5–0.6 µs | 0.6–0.7 µs |
| 5a | 2.9 ± 0.6 | 5.9 ± 1.0 | 0.5 ± 1.0 | 11.4 ± 0.7 | 6.0 ± 0.9 |
| 5b | - | 2.7 ± 0.7 | 3.7 ± 0.7 | 10.8 ± 0.7 | 1.1 ± 0.8 |
| 5c | - | - | 3.1 ± 0.5 | - | - |
| 5d | - | 2.6 ± 0.5 | 8.8 ± 0.7 | 3.1 ± 0.8 | - |
| 5e | - | - | - | 2.6 ± 0.5 | - |
| 5f | - | 1.5 ± 0.7 | 5.1 ± 0.8 | - | - |
| 5g | - | - | 7.1 ± 0.7 | 6.6 ± 0.8 | - |
| 5h | 2.7 ± 0.5 | 3.9 ± 0.8 | 3.5 ± 0.9 | 12.6 ± 1.0 | 9.0 ± 1.2 |

For Peer Review Only

Table 4: Summary of crack velocity measurements near or above $c_R$ in diamond. 'Successive measurements' refers to the number of interframe velocities measured over adjacent 100 ns intervals in high-speed sequences.

| Crack | Successive Measurements | Average Velocity (mm µs$^{-1}$) | Shown in Figure |
|---|---|---|---|
| 1a | 2 | $10.5 \pm 0.9$ | 3(a) |
| 2a | 1 | $12.2 \pm 1.4$ | 3(b) |
| 3a | 1 | $14.1 \pm 1.1$ | 3(c) |
| 5a | 1 | $11.4 \pm 0.7$ | 3(d) |
| 5b | 1 | $10.8 \pm 0.7$ | 3(d) |
| 5h | 2 | $10.8 \pm 0.8$ | 3(d) |

For Peer Review Only

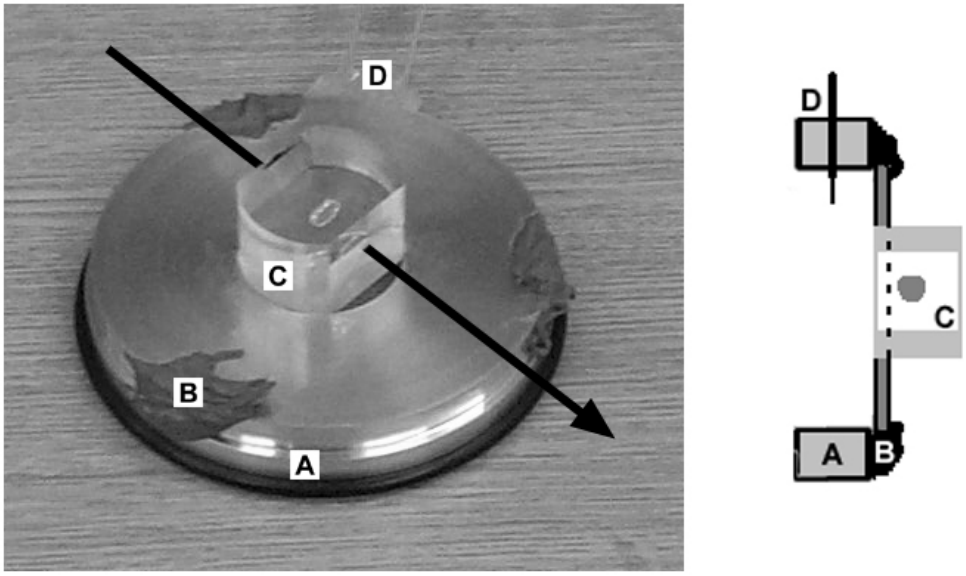


Figure 1: An embedded diamond specimen is photographed (left) with an arrow indicating the line of view for the high-speed camera. A schematic cross-section of the specimen (right) is shown from the viewpoint of the camera; the flyer plate arrives from the left in this diagram. Labelled features are:

(A) Aluminium alignment ring, thickness 15 mm, inner diameter 55 mm.

(B) Chemical metal epoxy, holding a 2 mm thick aluminium plate in place.

(C) Cylindrical polymer block, flush with the impact face, diameter 30 mm and thickness ∼15 mm. Two flat polished faces for photography are ∼20 mm apart. Embedded diamonds were emplaced ∼3 mm from the impact face.

(D) 'Make' trigger; two wires protrude through holes drilled into the alignment ring ∼3 mm from the impact face. The actual positions of the embedded diamond and the make trigger were measured to within ± 0.1 mm.

Review Only

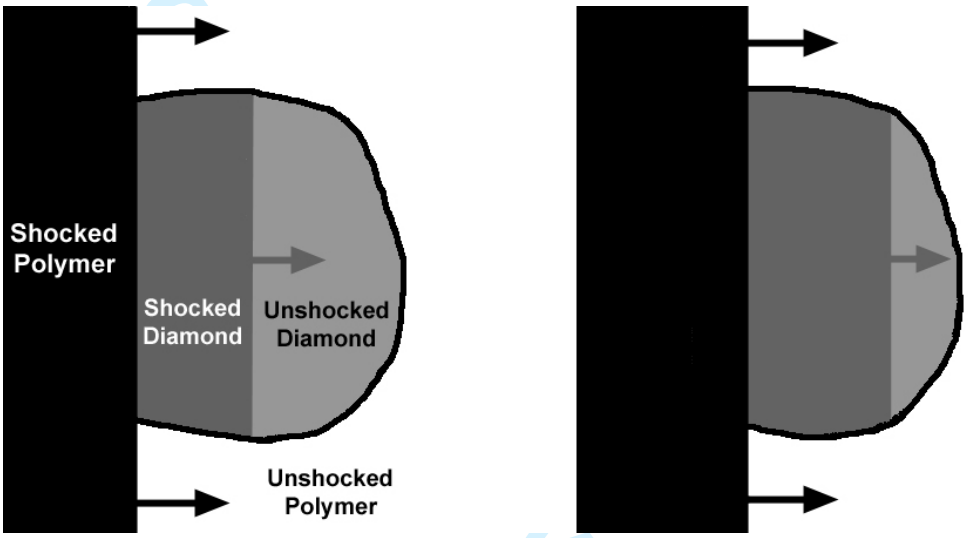


Figure 2: Two successive, schematic frames from a high-speed sequence showing the relative positions of shock waves and their effect on the imaging of an embedded diamond specimen. The 'window' is that part of the diamond that is unobscured by the shock in the polymer. In some experiments, the dark band in the polymer is thin enough for the diamond to be observed after the leading edge of the shock wave has passed.

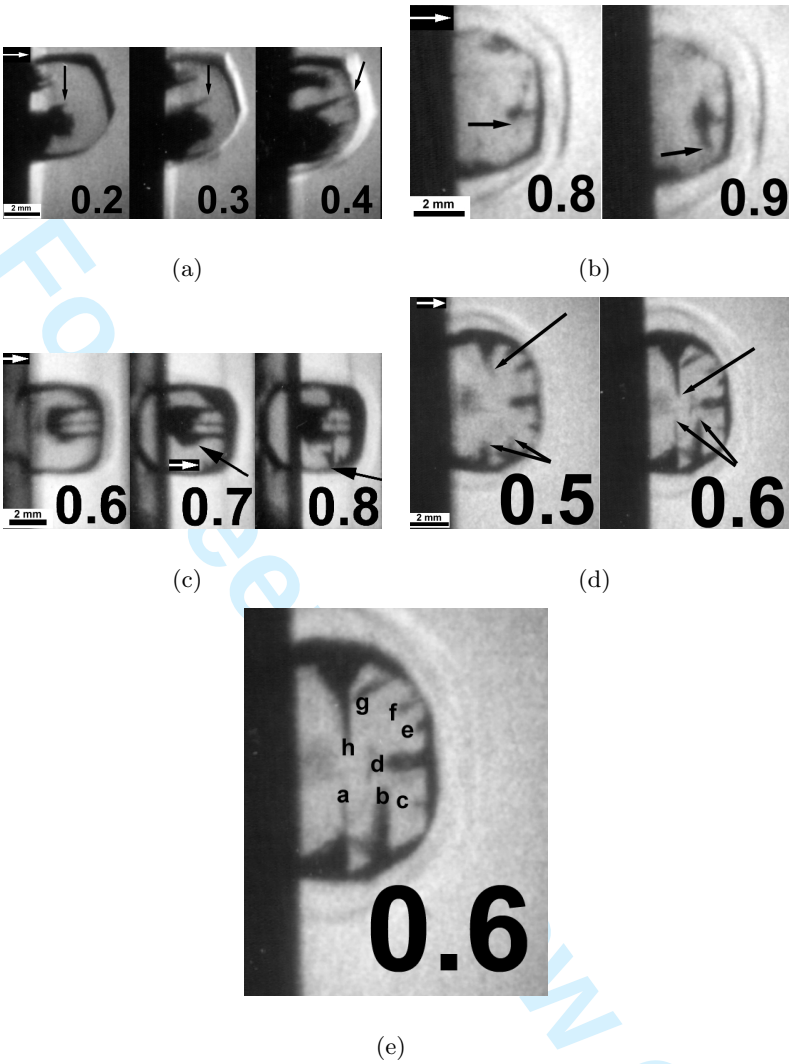


Figure 3: Frames from four high-speed sequences, with propagating fast cracks (table 4) denoted by arrows. The white arrow in the first frame of each sequence points to the edge of the dark, vertical shock front in the PMMA matrix. Each frame is labelled with the time in microseconds after shock wave arrival. Figures 3(a), 3(b), 3(c) and 3(d) show frames from experiments D1, D2, D3 and D5 respectively; experimental details are recorded in table 2. The white arrow in the second frame of figure 3(c) is discussed in the text. Figure 3(e) shows the labels for eight cracks in experiment D5, with velocities recorded in table 3.

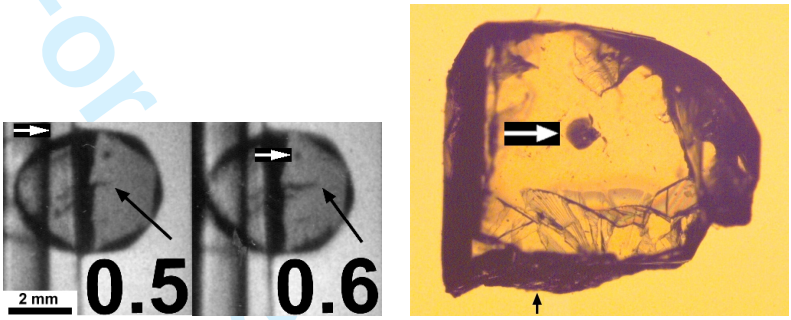


(a) (b)

Figure 4: Figure 4(a) shows frames from the high-speed sequence for experiment D8, with each frame labelled with the time in microseconds after shock wave arrival. A white arrow in the first frame points to the edge of the dark, vertical shock front in the PMMA matrix. The specimen was only partially embedded in PMMA: the second vertical line, to the right of the shock front, is the edge of the PMMA matrix. Experimental details are recorded in table 2. Figure 4(b) shows a diamond fragment recovered from experiment D8. A near-circular inclusion in the specimen is indicated by white arrows in figure 4(b) and the second frame of figure 4(a). The propagating crack that is denoted by arrows in Figure 4(a) creates the fracture surface next to the arrow in Figure 4(b).

For Peer Review Only

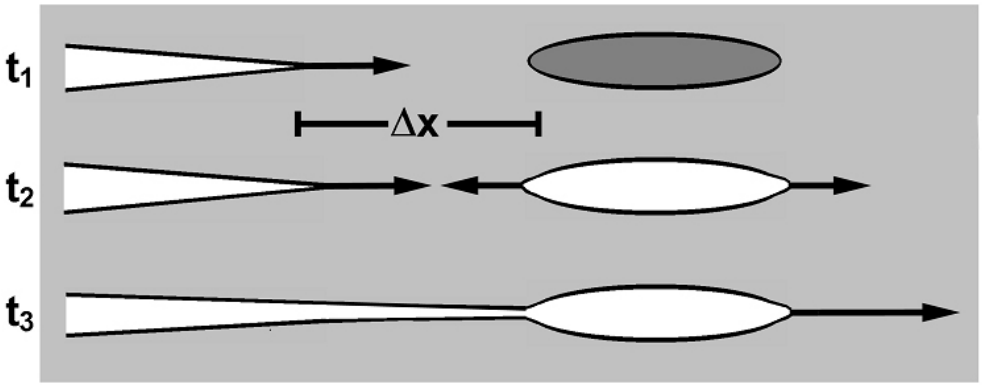


Figure 5: Schematic description of the multiple initiation mechanism for extension of fracture surfaces. Arrows indicate propagating crack tips. Initially ($t_1$), a primary crack propagates towards a static flaw on the same {111} cleavage plane at velocity $v$. When the separation of the flaw and the primary crack tip is $\Delta x$, the flaw extends into secondary cracks that move in both directions along the cleavage plane ($t_2$). The primary and secondary cracks eventually coalesce into one fracture ($t_3$). If the intermediate step is not observed, the crack appears to travel faster than $v$.